Sustainable Chemical Engineering
https://ojs.wiserpub.com/index.php/SCE/

Research Article

Plant-Derived Lignocellulose Frameworks Functionalized with Silver Nanoparticles for Antimicrobial Applications

Anil Sigdel[1], Arun Kumar Sharma[1], Naresh Prashad Pant[1,2], Basanta Subedi[1], Hari Bhakta Oli[1*], Deval Prasad Bhattarai[1†]

[1]Department of Chemistry, Amrit Campus, Tribhuvan University, Kathmandu, 44618, Nepal
[2]School of Materials Science and Engineering, University of Science and Technology of China, Shenyang, 110016, China
E-mail: hari.oli@ac.tu.edu.np, deval.bhattarai@ac.tu.edu.np

Received: 14 April 2026; **Revised:** 6 May 2026; **Accepted:** 15 June 2026

Graphical Abstract:

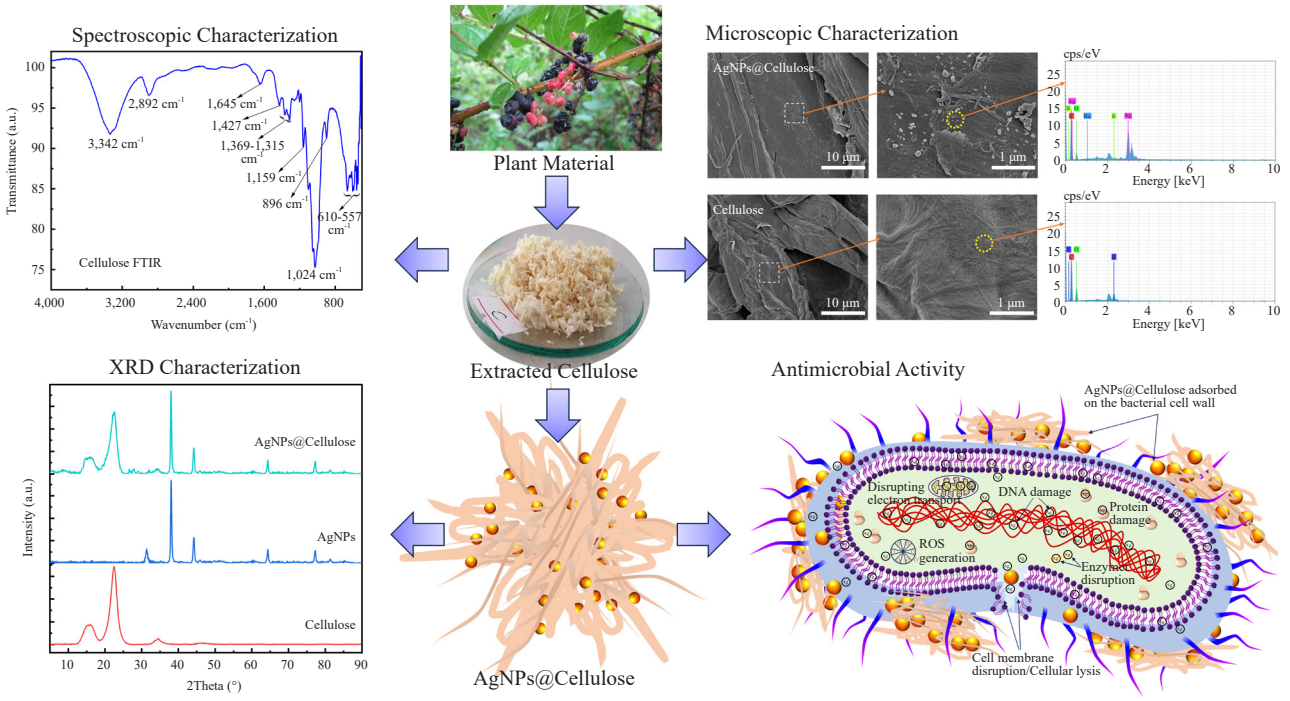

Abstract: Lignocellulosic biomaterials represent the most abundant renewable polymeric resources in nature and serve as sustainable potential alternatives to synthetic polymers due to their biodegradability, renewable sourcing, eco-friendly processing, and cost-effectiveness. In this study, cellulose, hemicellulose, and lignin were successfully extracted from the stems of *Alnus nepalensis* and *Coriaria nepalensis* and subjected to comprehensive physicochemical characterization. Quantitative compositional analysis of the biomasses revealed cellulose contents of 37% and 25.53%

DOI: https://doi.org/10.37256/sce.72202610014

in *Alnus nepalensis* and *Coriaria nepalensis*, respectively. Similarly, hemicellulose yields were 8.70% and 9.41%, while lignin contents were significantly lower, with the measured values of 1.8% and 0.1% for the respective species. The extracted lignocellulosic components were characterized using chemical analysis, Fourier Transform Infrared Spectroscopy (FTIR), X-Ray Diffraction (XRD), and Scanning Electron Microscopy coupled with Energy-Dispersive Spectroscopy (SEM/EDS). Furthermore, Silver Nanoparticles (AgNPs) were synthesized and effectively incorporated within the cellulose matrix. Antimicrobial evaluation demonstrated significant inhibitory activity against the Gram-negative bacterium *Escherichia coli*, whereas no appreciable effect was observed against Gram-positive *Bacillus subtilis.* These findings underscore the potential of lignocellulosic biomaterials from these plant species for sustainable polymer applications and functional nanocomposites.

***Keywords*:** *Alnus nepalensis*, *Coriaria nepalensis*, cellulose, hemicellulose, lignin

1. Introduction

Recent discourse on natural resource preservation and sustainable waste management has reignited scientific interest in natural materials, particularly those derived from renewable sources. Among these, natural polymer materials have sparked significant attention due to their ecological advantages and potential applications.[1] Lignocellulosic biomass, recognized as the most abundant renewable resource globally, presents considerable promise for the production of value-added chemicals and advanced biomaterials.[2,3] Against the backdrop of growing environmental concern, lignocellulosic materials and industrial solid wastes with high cellulose content have emerged as focal points in sustainable materials research.[4]

Cellulose, a major structural constituent of plant cell walls and vegetable fibers, is an insoluble white crystalline polysaccharide. As one of the most abundant renewable natural polymers, it is widely regarded as an inexhaustible raw material owing to its extensive availability.[5,6] Major sources of cellulose include agricultural wastes, lignocellulosic biomass, and industrial solid wastes.[4,6] Chemically, cellulose is a polysaccharide composed of linear chains of β(1→4)-linked D-glucose units.[7,8] Its molecular formula, $(C_6H_{10}O_5)_n$, denotes a seemingly simple polymeric structure; however, these linear chains exhibit a high degree of polymerization and assemble into robust microfibrils through extensive hydrogen bonding interactions.[9,10] Cellulosic fibers are formed by the aggregation of approximately 40 cellulose microfibrils into a bundle, which are further embedded within a matrix of lignin and hemicellulose.[11] The hierarchical microfibrillar structure (Figure 1) imparts cellulose with outstanding mechanical strength and rigidity.[12,13] Historically, cellulose has been utilized in construction materials, papermaking, textiles, and apparel, primarily derived from wood and plant fibers.[5] Its notable properties, such as biodegradability, recyclability, renewability, biocompatibility, high resistivity, rigidity, superior tensile strength, low coefficient of thermal expansion, and high Young's modulus, render it a highly versatile material.[4,8] Importantly, the mechanical and chemical properties of cellulose are contingent upon its structural form and source.[5]

Hemicelluloses are structurally simpler polysaccharides compared to cellulose, consisting of heteroglycans composed of diverse sugar units with varying substituents.[14] These branched polymers include xylose, galactose, mannose, arabinose, and their corresponding uronic acids.[1] Hemicelluloses form hydrogen bonds with cellulose, contributing to the structural integrity of plant cell walls. Due to their functional versatility, hemicelluloses are employed in packaging, hydrogels, cosmetics, thermoplastics, adhesives, and pharmaceuticals as drug delivery agents.[15] Lignin acts as a structural binder between cellulose and hemicellulose, imparting rigidity and hydrophobicity.[16] Its amorphous three-dimensional structure is highly complex, with softwood lignin primarily composed of coniferyl alcohol units, while hardwood lignin contains both coniferyl and sinapyl alcohols.[17] Lignin forms covalent linkages with hemicellulose through benzyl-ether, phenyl glycosides, and benzyl-ester bonds, resulting in lignin-carbohydrate complexes.[18] Owing to its unique physicochemical properties, lignin finds applications in emulsifiers, dyes, synthetic flooring, sequestering agents, binders, thermosetting resins, dispersants, paints, biofuels, and road stabilization materials.[16] Given the overwhelming number of applications, the separation of lignocellulosic components from plant fibers is of great importance. Among the lignocellulose, the unique combination of strength and flexibility makes cellulose valuable for paper manufacturing. Beyond conventional writing paper, cellulose finds extensive applications in diverse sectors, including textile production (cotton-based fabrics), printing media, packaging materials, decorative papers, security

documents, currency production, and various industrial processes.[19,20] The papermaking process utilizes cellulose derived from both softwood species (e.g., spruce, pine, fir, larch, etc.) and hardwood species (e.g., eucalyptus, aspen, birch, etc.).[21] In the context of Nepal, indigenous plant species, including *Eulaliopsis binata*, *Bambusa vulgaris*, and *Daphne panachea*, have been traditionally employed in the production of Nepali Kagaj (paper).[22,23] The distribution and availability of these paper-making species have been documented; however, a comprehensive study to analyze cellulose composition across different plant materials remains lacking and is of urgent need to establish the industry. This study specifically determines the cellulose content in stems of two Nepalese plant species of the Betulaceae family: *Alnus nepalensis* and *Coriaria nepalensis* (Figure 2(a, b)), addressing a significant gap in our understanding of their potential for paper production.

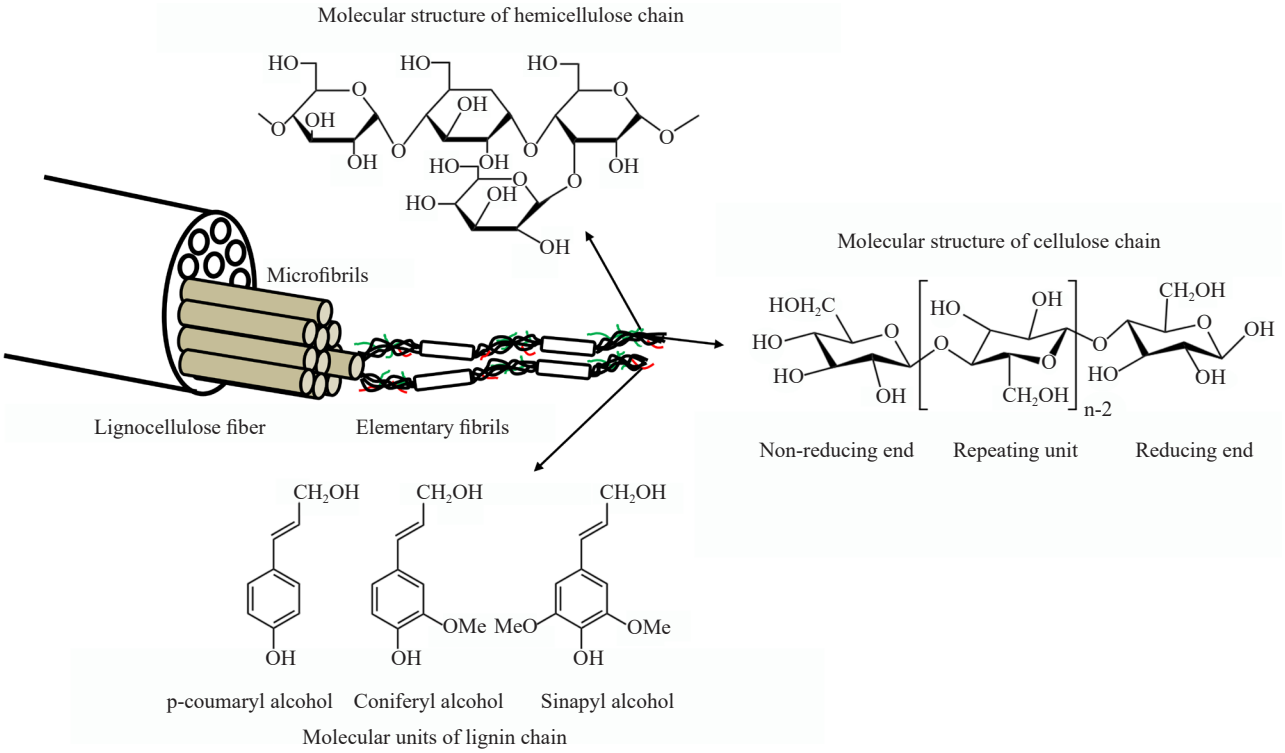

Figure 1. Molecular structure of cellulose, hemicellulose, and lignin in lignocellulose fiber[12,13]

Alnus nepalensis (commonly known as Uttis in Nepali) is a pioneer tree species predominantly found in subtropical highland ecosystems of the Himalayan region. The species exhibits a broad altitudinal distribution across Nepal, ranging from 200 to 3,030 meters above sea level.[24] This multipurpose deciduous tree possesses several ecologically and economically valuable attributes, including rapid growth rates, nitrogen-fixing capabilities through symbiotic actinorhizal associations, and utility as a source of moderately soft timber and charcoal feedstock.[25] The xylem structure of *A. nepalensis* demonstrates considerable anatomical plasticity, with distinct altitudinal variations observed in several key morphological characteristics. *Coriaria nepalensis* (commonly known as *Machhaino* in Nepali) is a deciduous shrub species exhibiting a broad ecological distribution across Nepal, occurring at elevations ranging from 400 to 3,200 meters above sea level. Current investigations have demonstrated significant antimicrobial and antifungal properties in both essential oil constituents and methanol extract.[26,27] Despite these documented bioactive properties, *C. nepalensis* remains largely undervalued in economic terms and is frequently categorized as an invasive weed species due to its competitive interference with both agricultural and forestry operations.[28] This perception has limited the exploration of its potential commercial applications.

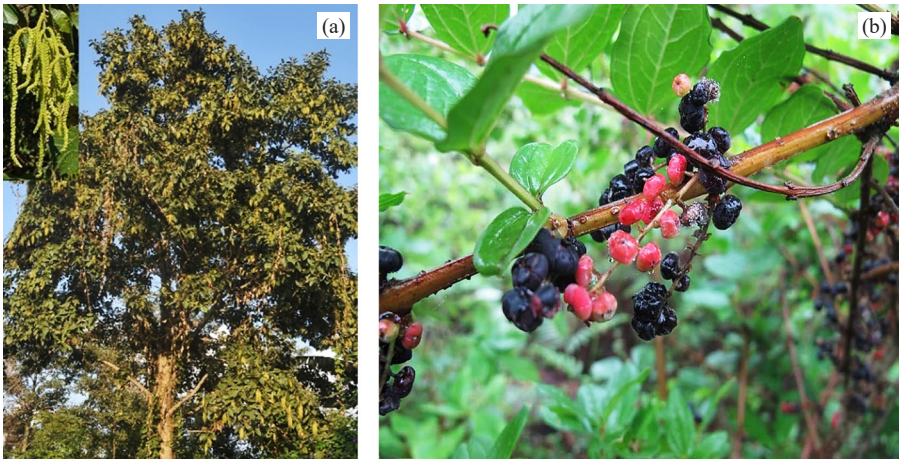

Figure 2. (a) *Alnus nepalensis* tree and flower; (b) *Coriaria nepalensis* fruit twig

Notably, previous studies in this field exhibit critical gaps and limitations that underscore the novelty and importance of the present work. While prior research has established the value of lignocellulosic biomass for sustainable materials and papermaking, and documented the traditional use of some indigenous Nepalese plant species in Nepali Kagaj production,[22,23] comprehensive analyses of cellulose composition across diverse local plant materials are lacking. This knowledge gap hinders the sustainable development of Nepal's domestic paper industry, as cellulose content is a key determinant of a plant's suitability for papermaking. Additionally, species such as *C. nepalensis* have been documented to possess bioactive properties[26,27] but remain economically undervalued and misclassified as invasive weeds,[28] with no prior exploration of their lignocellulosic potential. Most existing research also focuses on globally common softwood and hardwood species[21] rather than region-specific Nepalese species like *A. nepalensis* and *C. nepalensis*, which could be better adapted to local ecological and industrial conditions.

Comparing the materials studied herein to similar alternatives further highlights the relevance of this work. Unlike traditional Nepalese papermaking plants (e.g., *Eulaliopsis binata*, *Bambusa vulgaris*), *A. nepalensis* (a fast-growing, nitrogen-fixing pioneer tree) and *C. nepalensis* (a widely distributed shrub) represent untapped feedstocks; comparing their cellulose content to these traditional species will reveal their potential as alternative or complementary resources, with potential advantages such as faster growth or broader ecological adaptability. Relative to globally common papermaking materials (e.g., spruce, eucalyptus),[21] quantifying cellulose in *A. nepalensis* and *C. nepalensis* will determine if these Nepalese species can match or supplement the cellulose yields of global species, offering insights into their competitiveness as local, renewable alternatives that reduce reliance on imported feedstocks.

The unique features and core goals of this study are clearly defined to address these gaps. This work is the first to specifically quantify cellulose content in the stems of *A. nepalensis* and *C. nepalensis*, two understudied Nepalese species, to evaluate their potential for papermaking, prioritizing locally available, ecologically adapted species over globally common ones. Beyond mere cellulose quantification, the study aims to challenge the misclassification of *C. nepalensis* as a mere invasive weed by highlighting its potential as a renewable feedstock and exploring *A. nepalensis's* suitability for papermaking, leveraging its ecological benefits (nitrogen fixation, rapid growth) to promote sustainable, circular biomass utilization in Nepal. The overarching goal is to fill the critical gap in understanding the cellulose composition of these two species, providing empirical data to support the sustainable development of Nepal's domestic paper industry by identifying new, local feedstocks that are both ecologically viable and economically valuable. In doing so, this work aligns with global priorities for sustainable waste management and natural resource conservation while leveraging Nepal's indigenous biodiversity, further emphasizing its novelty and importance.

2. Materials and methods

2.1 Chemicals and instruments

All the chemicals: H_2SO_4 (Thermo Fischer Scientific, sp.gr. 1.835, purity 97%), oxalic Acid (Thermo Fischer Scientific India Pvt. Ltd, Molecular weight 126.07, purity 99%), NaOH (Merck life Science, Molecular weight 40, purity 97%), Methanol (Thermo Fischer Scientific India Pvt. Ltd, Molecular wt. 32.04, sp.gr. 0.792), glacial acetic acid, nitric acid, ethanol, toluene, formic acid, hydrogen peroxide were used in as-received form without purification. Instruments like Ultraviolet-Visible (UV) Spectrophotometer (Labtronics, LT-2802), Fourier Transform Infrared Spectroscopy (FTIR) (Perkin Elmer 10.6.2), and Rota evaporator (IKA 10) were used in this work.

2.2 *Sampling of plant stems and processing*

The stem samples with intact bark were collected from two distinct mountainous regions of Nepal: *Alnus nepalensis* from Melamchi (27.9512° N, 85.6846° E; 1,275 m elevation), Sindhupalchok district, and *Coriaria nepalensis* from Bagarkot (29.1754° N, 80.2759° E; 1,257 m elevation), Dadeldhura district (Figure 3). Following collection, stems were sectioned into small pieces (≈ 5 cm) after removing the bark, thoroughly washed with distilled water, and shade-dried for 15 days at a humidity level of 43-45% at ambient temperature. The dry stems were then mechanically ground into powder using an herbal medicine disintegrator (FW177). The resulting powder was sieved through a 250 µm sieve and stored in an airtight glass vial under dry conditions until processing.

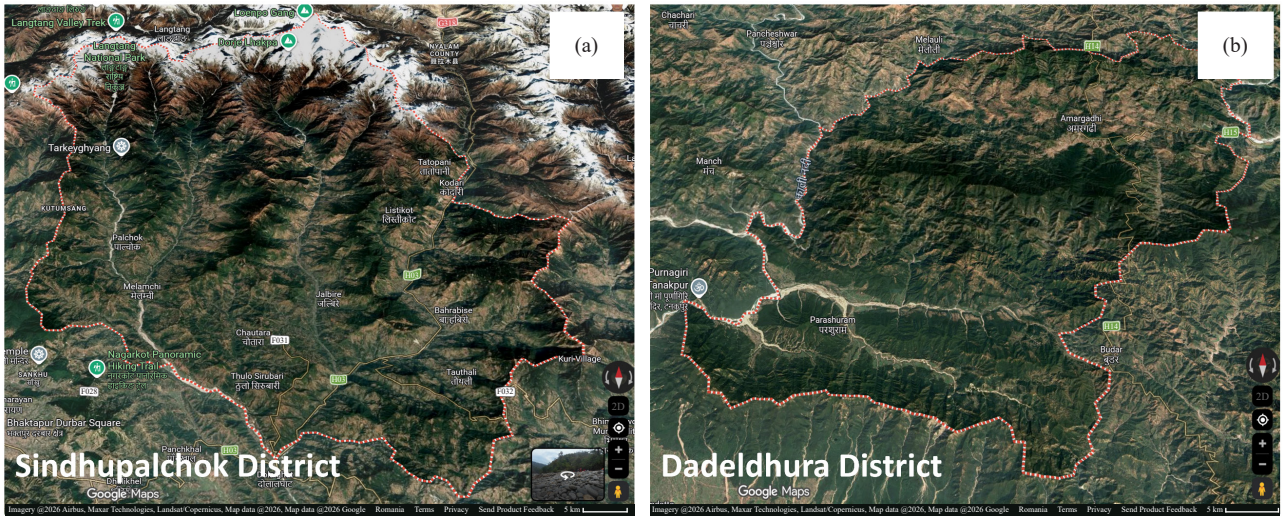

Figure 3. Google map of sample collected sites: (a) Sindhupalchok district and (b) Dadeldhura district

2.3 *Cellulose extraction*

The cellulose extraction protocol followed a sequential purification process comprising the removal of extractives, pre-alkalization, alkalization, acetylation, and acid hydrolysis.[4] Initially, 5 g of powder from each plant sample was placed in separate beakers and treated with ethanol/benzene solution (1 : 2 v/v, 45 mL total volume) at ambient temperature for 24 hours, followed by the removal of supernatant. The content was thoroughly washed with distilled water and dried in an oven at 80 °C for 6 h. Subsequent alkaline treatments involved immersion in 2.5% (w/v) NaOH for 24 hours, followed by reflux extraction with 7.5% (w/v) NaOH for 90 minutes to solubilize hemicellulose and lignin fractions. Neutralized residues (pH 7-8 achieved through distilled water washing) underwent acid hydrolysis using acetic/nitric acid (6 : 1 v/v, 25 mL/sample) for 30 minutes, with subsequent neutralization to pH 6. The acetylated cellulose was then treated with 32% sulphuric acid at 45 °C for 30 min under constant agitation, and the reaction was

terminated by dilution with distilled water. The resulting suspension was aged for 48 hours, vacuum-filtered through a pre-weighed glass crucible, and oven-dried at 45 ± 5 °C to a constant weight. For quantitative analysis, triplicate extractions were performed under identical conditions to ensure methodological reproducibility and enable calculation of mean extraction yields.

2.4 *Hemicellulose extraction*

The hemicellulose fraction was isolated using an alkaline extraction protocol.[15] Following initial delignification, samples were subjected to NaOH treatment at varying concentrations with constant mechanical agitation at 50 °C for 3 hours to facilitate hemicellulose solubilization. The resulting suspension was vacuum-filtered through Whatman No. 1 filter paper, and the filtrate pH was adjusted to 5-6 by adding acetic acid. Ethanol precipitation was performed at 4 °C, with the mixture allowed to stand for 48 hours to ensure complete precipitation of hemicellulose. After decanting the supernatant, the precipitated hemicellulose was washed three times with 70% ethanol and dried at 45 °C until constant weight was achieved.

2.5 *Lignin extraction*

Lignin isolation was conducted through a sequential process involving acid treatment, peroxy acid delignification, bleaching, and final precipitation.[16] Samples were initially refluxed with formic/acetic acid (70 : 30 v/v) at a 1 : 8 (w/v) solid-to-liquid ratio for 2 hours at 90 °C. The acid-insoluble residue was sequentially washed with formic acid and distilled water before undergoing peroxyacid treatment (peroxy-formic acid/peroxy-acetic acid, 1 : 1 v/v) in a temperature-controlled water bath at 80 °C for 2 hours. Subsequent bleaching was performed using peroxide solution under identical conditions. The filtrate was concentrated in an oil bath at 105 °C, with lignin precipitated by gradual addition of distilled water. The precipitated lignin was collected via vacuum filtration and air-dried at room temperature for 48 hours.

2.6 *Characterization of the extracted lignocellulose*

The extracted lignocelluloses were characterized using chemical, spectroscopic, crystallographic, and microscopic methods. Additionally, antimicrobial activities were also performed. In the chemical test method, extracted cellulose was treated with Schultze reagent ($KClO_3$ with varying amounts of concentrated HNO_3), and the violet coloration confirms the presence of cellulose. In the UV spectroscopic technique, absorbance shown by a suspension of cellulose and nanoparticle-incorporated cellulose in the UV range (300-550 nm) at a scan resolution of 5 nm was recorded using a UV double-beam spectrometer (Labtronics, LT2802), Amrit Campus, Kathmandu, Nepal. FTIR spectroscopic characterization of lignocellulosic materials was carried out using PerkinElmer Spectrum IR Version 10.6.2 operating in Attenuated Total Reflectance (ATR) mode, covering a range of 500-4,000 cm^{-1} at a scan interval of 4 cm^{-1} with a minimum of 50 measurement cycles. The X-Ray Diffraction (XRD) pattern of cellulose and nanoparticle-incorporated cellulose was obtained using an X-ray diffractometer (Rigaku, CuKα radiation, λ = 1.54 Å) at an operating voltage of 40 kV and current of 40 mA, with a scanning rate of 10° min^{-1} covering a range of 10-70°. The surface morphology of the cellulose and nanoparticles-incorporated cellulose was examined using a Field Emission Scanning Electron Microscope (FE-SEM) (Thermo Fischer, USA). Additionally, the incorporation of silver nanoparticles in cellulose matrix was ensured by Energy Dispersive X-ray (EDX) analysis, and elemental composition and distribution within the samples were determined.

2.7 *Silver Nanoparticles (AgNPs) incorporation into cellulose*

The Silver Nanoparticles (AgNPs) were synthesized via the chemical reduction method, for which 10 mL aqueous solution of 0.1 M $AgNO_3$ and the same volume of 0.1 M trisodium citrate were homogenized by magnetic stirring (300 rpm, 2 minutes) in a beaker. The reaction mixture was subsequently photo-reduced under ambient solar irradiation until a yellowish colloidal suspension formed, indicating nucleation of AgNPs. Meanwhile, 0.5 g of cellulose was dispersed separately in 20 mL of deionized water using ultrasonic treatment to achieve a uniform suspension. The cellulose

dispersion was then combined with the AgNPs colloidal solution and subjected to further solar irradiation for 24 hours, resulting in characteristic dark brown spots on the cellulose matrix indicative of successful incorporation of AgNPs onto cellulose. The final product was dried in sunlight to obtain dried nanoparticles.

2.8 *Antimicrobial test for AgNPs-cellulose*

The antimicrobial efficacy of the synthesized Silver Nanoparticles Incorporated Into Cellulose (AgNPs@CNC) was assessed using the standard paper disc diffusion assay. Two model bacterial strains were selected for evaluation: *Escherichia coli* American Type Culture Collection (ATCC) 8739 (Gram-negative) and *Bacillus subtilis* ATCC 6051 (Gram-positive). Bacterial inocula were prepared from fresh nutrient agar slant cultures and aseptically inoculated onto Mueller-Hinton agar plates. In the disc, 5 µg of AgNPs@CNC and 5 µg of reference antibiotic kanamycin were loaded separately. All plates were incubated at 37 °C for 24 hours under aerobic conditions. Following incubation, the Zones of Inhibition (ZOI) were measured using digital calipers (± 0.1 mm precision). Antimicrobial activity was quantified by comparing the mean inhibition zone diameters of test samples against control values, with measurements performed in triplicate to ensure statistical reliability.

3. Results and discussions

3.1 *Visual observation and chemical characterization*

The extracted lignocelluloses were inspected by visual observation; white fibers of cellulose (Figure 4a), dark brown powder of hemicellulose (Figure 4b), and light brown color of lignin (Figure 4c) were obtained. The chemical treatment of cellulose with the Schultze reagent displayed blue-violet coloration (Figure 4d), indicating the presence of cellulose.

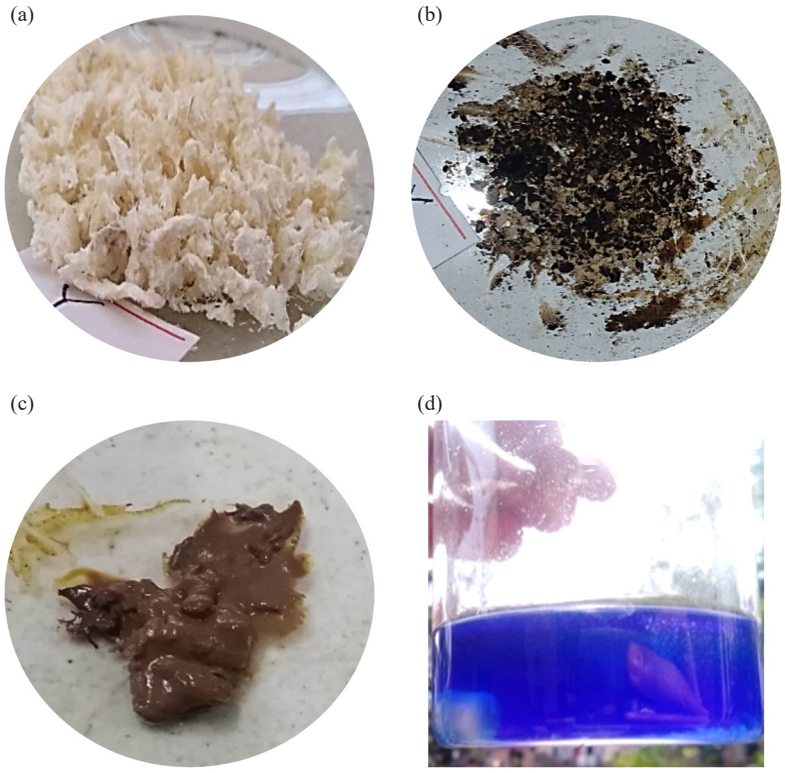

Figure 4. Lignocellulose mass: (a) Extracted cellulose, (b) Extracted hemicellulose, (c) Extracted lignin, and (d) blue-violet coloration of cellulose with Schultze reagent

3.2 *Quantitative analysis*

Quantitative determination of dry lignocellulosic materials was performed, for which the weight of lignocellulosic materials was measured by a 4-digit weighing machine (model, company, precision: ± 0.0001 g). Average weights and their corresponding percentages are presented in Figure 5(a) and (b), respectively. *Alnus nepalensis* species contains 37% cellulose, 8.73% hemicellulose, and 1.844% lignin, whereas for *Coriaria nepalensis*, they are 25.53%, 9.40%, and 1.14%, respectively.

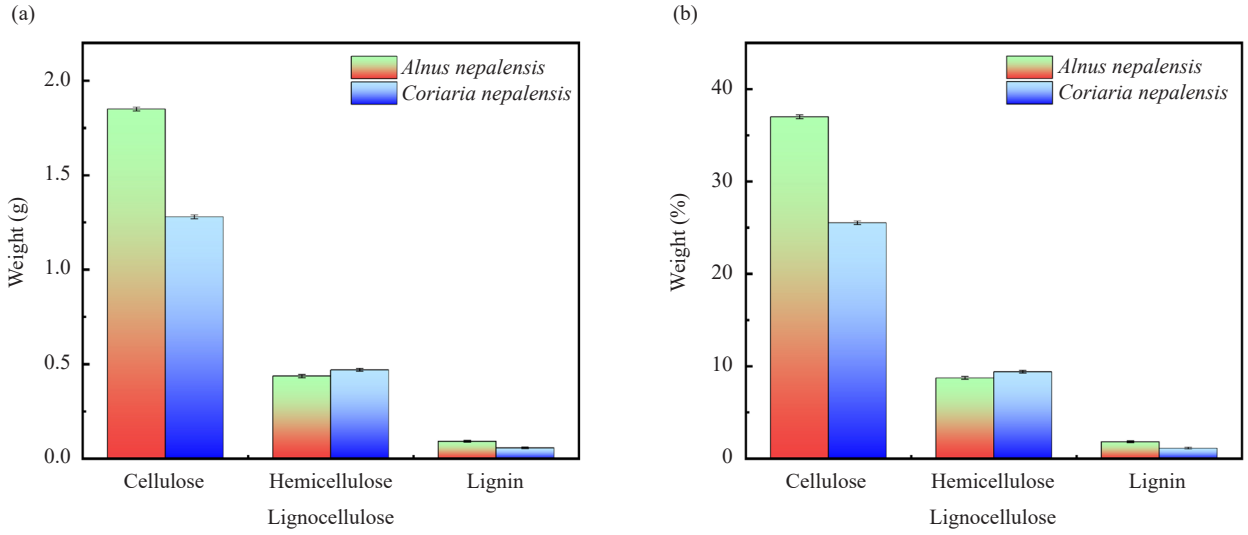

Figure 5. (a) average weight of lignocellulose obtained and (b) % yield of lignocellulose

3.3 *FTIR characterization*

The FTIR spectra of Cellulose isolated from *Alnus nepalensis* (ANC) and *Coriaria nepalensis* (CNC) exhibited characteristic absorption bands corresponding to functional groups present in cellulosic materials, as presented in Figure 6(a). Both samples displayed prominent absorption features in the 3,660-2,900 cm^{-1} region, with the broad band at 3,340 cm^{-1} (ANC) and 3,337 cm^{-1} (CNC) attributed to O-H stretching vibrations of hydroxyl groups in the polysaccharide matrix.[29,30] The distinct peaks at 2,899 cm^{-1} (ANC) and 2,897 cm^{-1} (CNC) represent C-H stretching vibrations of methylene groups in the cellulose polymer backbone. A notable absorption band at approximately 1,645 cm^{-1} in both spectra corresponds to the bending vibration of adsorbed water molecules within the cellulose structure. The fingerprint region (1,500-900 cm^{-1}) revealed several characteristic cellulose absorptions: 1,428 cm^{-1} (CH_2 bending), 1,354-1,358 cm^{-1} (C-H deformation), ~ 1,168 cm^{-1} (C-O-C antisymmetric bridge stretching), ~ 1,115 cm^{-1} (ring asymmetric stretching), and ~ 1,032 cm^{-1} (C-O stretching). The band at 897 cm^{-1}, present in both spectra, is indicative of β-glycosidic linkages between glucose units in cellulose.[30,31] Crystallinity analysis based on FTIR spectra revealed that the relative intensity of the 1,420-1,430 cm^{-1} band corresponds to the crystalline cellulose content, while the 897 cm^{-1} band represents the amorphous region, consistent with established literature.[30] The observed spectral similarities between ANC and CNC suggest comparable chemical compositions and structural features in the cellulose derived from both plant sources.

The FTIR spectra of Hemicellulose extracted from *Alnus nepalensis* (ANHC) and *Coriaria nepalensis* (CNHC) exhibited characteristic absorption patterns consistent with heteropolysaccharide structures, as shown in Figure 6(b). A broad absorption band centered at 3,379 cm^{-1} (ANHC) corresponds to –O-H stretching vibrations from hydroxyl groups present in the constituent sugar monomers. Distinct C-H stretching vibrations of methylene groups were observed at 3,243 cm^{-1} (ANHC) and 3,259 cm^{-1} (CNHC), demonstrating variations in side-chain conformations between the two samples. The spectra revealed characteristic deformation modes at 1,575 cm^{-1} and 1,410 cm^{-1} for ANHC, and 1,568 cm^{-1}

and 1,404 cm^{-1} for CNHC, corresponding to -CH_2 bending vibrations of xylose and other pentose units. A prominent absorption band at 1,038 cm^{-1} in both samples represents the combined contributions of C-O-C pyranose ring stretching and C-C skeletal vibrations, indicative of polysaccharide backbone structure. The diagnostic band at 897 cm^{-1} (ANHC) confirms the presence of β-(1→4) glycosidic linkages characteristic of hemicellulose polymers.[1,30,32] Spectral variations between ANHC and CNHC in the 1,500-1,300 cm^{-1} region suggest differences in acetylation patterns and side-chain substitutions, consistent with the known structural diversity of hemicelluloses across plant species.[30] The observed absorption profiles confirm successful isolation of hemicellulose fractions while demonstrating species-specific structural variations in these heteropolysaccharides.

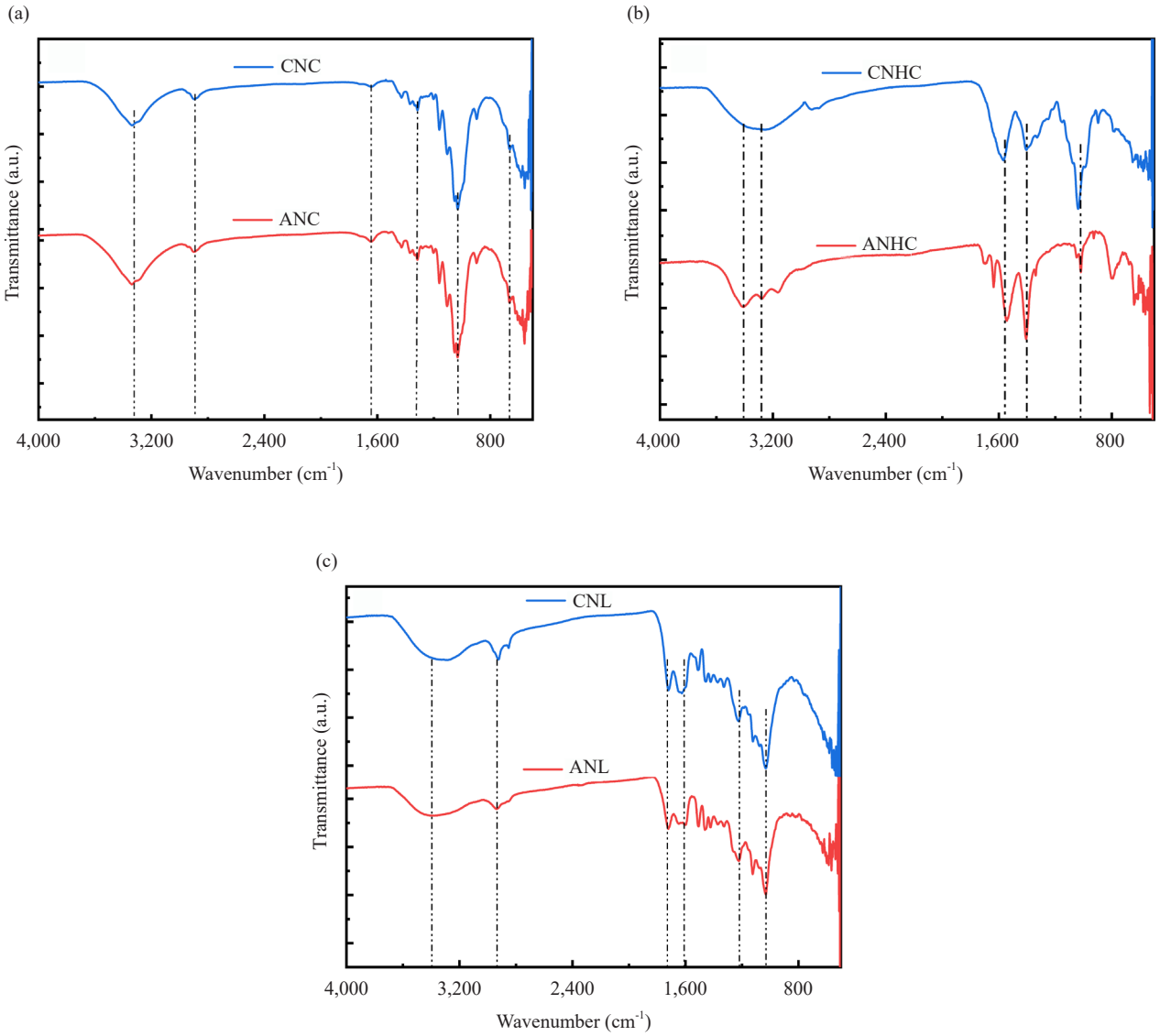

Figure 6. FTIR spectra of lignocellulosic mass: (a) Cellulose extracted from *Alnus nepalensis* stem (ANC) and *Coriaria nepalensis* stem (CNC), (b) Hemicellulose extracted from *Alnus nepalensis* stem (ANHC) and *Coriaria nepalensis* stem (CNHC), and (c) Lignin extracted from *Alnus nepalensis* stem (ANL) and *Coriaria nepalensis* stem (CNL)

The FTIR spectra of Lignin extracted from *Alnus nepalensis* (ANL) and *Coriaria nepalensis* (CNL) exhibited characteristic absorption bands corresponding to aromatic and aliphatic functionalities, as shown in Figure 6(c). A broad absorption band at 3,410 cm^{-1} (ANL) and 3,296 cm^{-1} (CNL) is attributed to –O-H stretching vibrations of

phenolic and aliphatic hydroxyl groups, demonstrating vibrations in hydrogen bonding networks between the two lignin samples. Distinct C-H stretching vibrations of methylene groups are observed at 2,938 cm^{-1} (ANL) and 2,923 cm^{-1} (CNL), confirming the presence of aliphatic side chains. The absorption bands at 1,722 cm^{-1} (ANL) and 1,720 cm^{-1} (CNL) correspond to C=O stretching of conjugated carbonyl/carboxyl groups, potentially originating from residual hemicellulose acetyl groups or oxidized lignin subunits. The fingerprint region reveals key structural features, such as absorption bands in between 1,328-1,223 cm^{-1} corresponding to aromatic C-C stretching and methoxyl C-H bending vibrations. Absorbance band at 1,032 cm^{-1} is characteristic C-O/C-C stretching of glycosidic linkages, indicative of residual xylan.[14,17,18,30] The observed spectral differences in the 1,300-1,200 cm^{-1} region suggest variations in guaiacyl/syringyl unit ratios between the two lignin samples, consistent with known interspecies differences in hardwood/softwood lignins.[14,30] These results confirm successful lignin isolation while highlighting structural variations between species.

3.4 *UV-visible characterization*

UV-visible spectroscopy serves as a primary characterization technique for evaluating the optical properties of both AgNPs and AgNPs@CNC. The synthesized AgNPs exhibited a characteristic Surface Plasmon Resonance (SPR) absorption band at 455 nm (Figure 7a), consistent with the typical SPR profile of colloidal silver nanoparticles. In contrast, the AgNPs@CNC displayed multiple absorption maxima at 400 nm, 460 nm, and 525 nm (Figure 7b). These observations align with the previous reports as reported by Nayem et al.[33] Also, the spectral profile closely matches the results obtained by Vijayakumar et al.,[34] using sodium borohydride-mediated synthesis, confirming the successful incorporation of AgNPs within the cellulose matrix. The observed bathochromic shifts and band broadening suggest strong nanoparticle-matrix interactions that modify the plasmonic properties of the incorporated AgNPs.

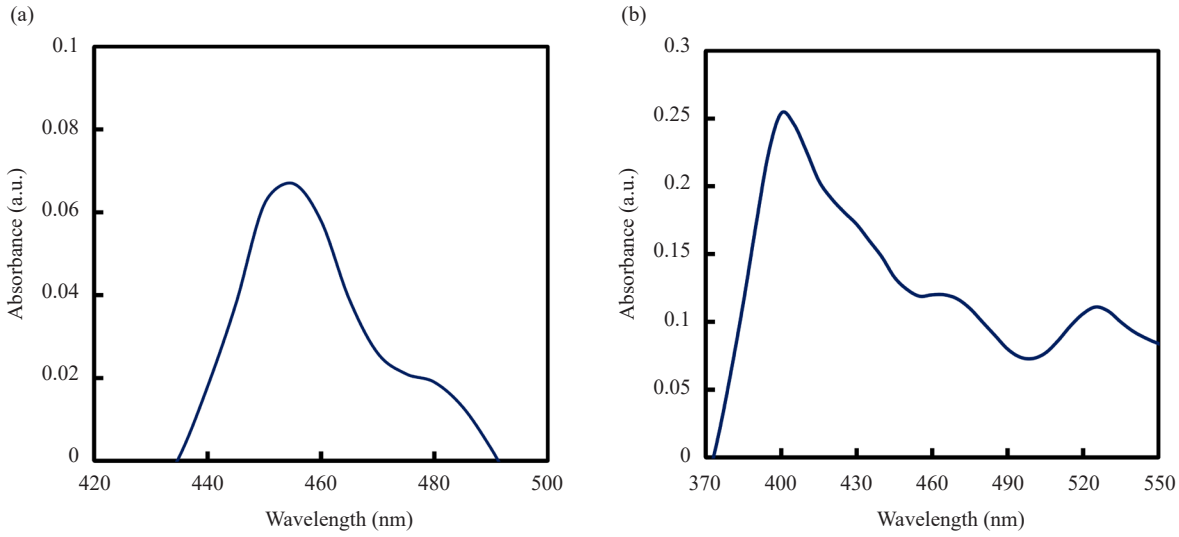

Figure 7. UV-Visible spectra of (a) Silver Nanoparticles (AgNPs) and (b) AgNPs Incorporated Into Cellulose (AgNPs@CNC)

3.5 *XRD characterization*

The X-ray diffraction profiles in Figure 8 compare the crystalline structures of pure AgNPs, isolated cellulose fractions (ANC and CNC), and their corresponding AgNPs-incorporated cellulose. X-ray diffraction analysis confirmed the crystalline nature of both cellulose and AgNPs@CNC materials. The cellulose matrix exhibited characteristic diffraction peaks (2θ) at 16°, 23°, and 34°, corresponding to the (110), (200), and (004) crystallographic planes of cellulose Iβ polymorph, respectively.[35-37] These reflections remained unshifted in the composite material, indicating preservation of the native cellulose crystal structure after AgNPs incorporation.

The AgNPs demonstrated Face-Centered Cubic (FCC) crystallinity, consistent with the Joint Committee on Powder Diffraction Standards reference (JCPDS 04-0783), with prominent reflections at 2θ values of 28° (210), 32.4° (122), 38° (111), 46.7° (231), 54.8° (200), 57.1° (220), and 65° (220).[37-39] The reflections at 27.5°, 54.8°, and 57.1° indicate partial surface oxidation, though these angles have been previously reported for metallic silver.[40,41] Application of the Debye-Scherrer equation to the (111) reflection yielded an average crystallite size of 14.23 nm for the AgNPs.

The diffraction pattern of AgNPs@CNC showed superposition of both cellulose and AgNPs reflections without peak shifting or broadening, demonstrating that: the cellulose crystalline structure remains intact after nanoparticle incorporation, AgNPs maintain their FCC crystalline structure, and the impregnation process does not induce structural defects in either component. These results confirm successful physical incorporation of crystalline AgNPs within the cellulose matrix while maintaining the structural integrity of both components.[37]

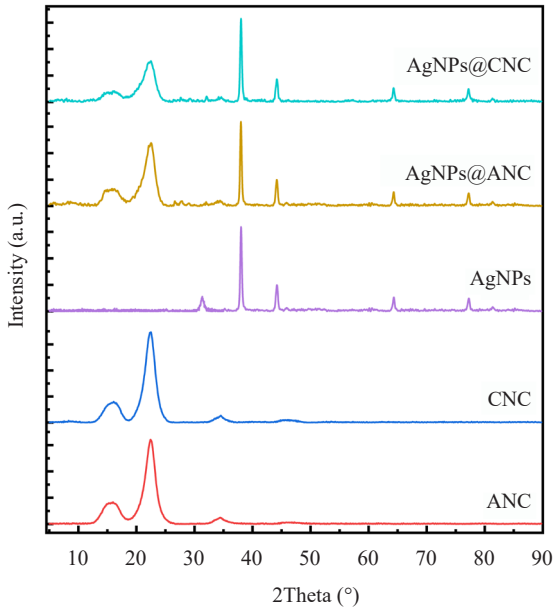

Figure 8. XRD pattern of AgNPs, ANC, CNC, AgNPs@ANC, and AgNPs@CNC

3.6 *SEM/EDS characterization*

Field-Emission Scanning Electron Microscopy coupled with Energy Dispersive X-ray Spectroscopy (FE-SEM/EDS) was employed to characterize the three-dimensional morphology and elemental composition of the cellulose materials and their silver nanocomposites. As shown in Figure 9(a-l), both native cellulose samples (ANC and CNC) exhibited characteristic nanofibrillar networks with interconnected fibers forming porous matrices, demonstrating similar structural organization regardless of plant source. EDS analysis confirmed the expected carbon and oxygen composition of cellulose, with trace sulfur impurities attributed to residual sulfate groups from the extraction process. The nanoparticles impregnated cellulosic materials (AgNPs@ANC and AgNPs@CNC) revealed homogeneous dispersion of silver nanoparticles across the cellulose fiber surface without disruption of the underlying fibrous architecture. EDS spectra of the composites showed distinct silver peaks alongside the cellulose matrix signals, confirming successful nanoparticle incorporation. Notably, the identical deposition patterns and nanoparticle distributions observed for both ANC and CNC-based composites indicate that the silver impregnation mechanism is independent of the cellulose source material. These findings collectively demonstrate the successful fabrication of silver-cellulose nanocomposites while preserving the structural integrity of both the biopolymer matrix and metallic nanoparticles. The consistent morphological features across samples further validate the reproducibility of both the cellulose extraction and

nanoparticle functionalization process.

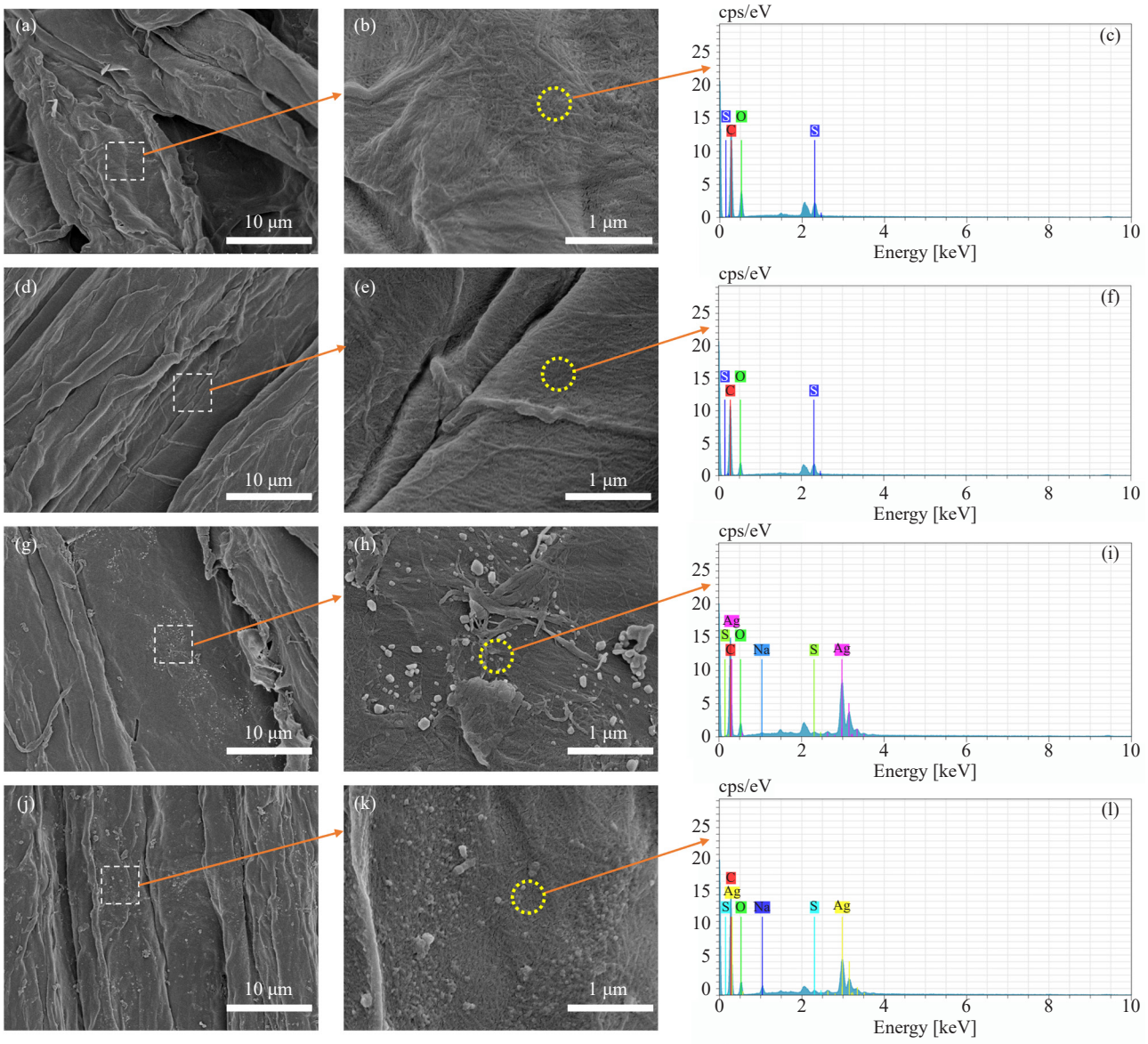

Figure 9. SEM and EDS spectra of CNCs and AgNPs@CNCs (a, b) *Alnus nepalensis* Cellulose (ANC), (c) EDS of ANC, (d, e) *Coriaria nepalensis* cellulose (CNC), (f) EDS of CNC, (g, h) AgNPs@ANC, (i) EDS of AgNPs@ANC, (j, k) AgNPs@CNC, and (l) EDS of AgNPs@CNC

3.7 *Antimicrobial activity*

The antimicrobial efficacy of AgNPs and their cellulose nanocomposites was evaluated against two American Type Culture Collection (ATCC) bacteria, Gram-positive *Bacillus subtilis* (ATCC 6051) and Gram-negative *Escherichia coli* (ATCC 8739), using the standardized paper disc diffusion assay. As presented in Table 1, both AgNPs and nanocomposites demonstrated significant Zones of Inhibition (ZOI) of 9.6, 7.4, and 7.1 mm, respectively, after 12 hours of incubation at 37 °C, with kanamycin (5 µg/disc) serving as the positive control (ZOI of 10.3 mm). Comparative analysis revealed that while pure AgNPs exhibited marginally larger inhibition zones, the nanocomposites maintained substantial antimicrobial activity, particularly against *E. coli*, where their performance was comparable to both AgNPs

and the antibiotic control. The slightly reduced efficacy (ZOI of 9.5, 4.5, and 4.3 mm for AgNPs, AgNPs@ANC, and AgNPs@CNC, respectively) observed against *B. subtilis* suggests that there are differential susceptibility patterns between Gram-positive and Gram-negative strains. These results confirm two critical findings: the successful retention of antimicrobial properties following AgNPs incorporation into the cellulose matrix and the controlled release of bioactive silver ions from the nanocomposite structure. The demonstrated antimicrobial performance, coupled with the structural advantages of cellulose-based delivery systems, positions these nanocomposites as promising candidates for antimicrobial applications in the medical and packaging industries. The variation in microbial susceptibility highlights the importance of target-specific optimization when developing such antimicrobial materials.

Table 1. Antimicrobial performance of AgNPs, AgNPs@ANC, and AgNPs@CNC against two selected bacterial strains

Strains	Zone of Inhibition (mm)			
	AgNPs	AgNPs@ANC	AgNPs@CNC	Standard Kanamycin
Escherichia coli (ATCC 8739)	9.6	7.4	7.1	10.3
Bacillus subtilis (ATCC 6051)	9.5	4.5	4.3	10.2

Based on these findings, it is revealed that AgNPs-cellulose nanocomposites exhibit substantial antimicrobial potential for biomedical and packaging applications. The study confirms preservation of AgNPs bioactivity within the cellulose matrix, which is of paramount importance for developing sustainable, controlled-release antimicrobial materials in the advanced biomedical and industrial applications. The major findings of this work are compared with existing literature in Table 2.

Table 2. Comparison of research findings of this work with existing literature

Source of cellulose	% of Cellulose	NPs impregnation	Antimicrobial activity (ZOI, mm)	Reference
Sisal Hemp Flex	> 30%	-	-	4
Wood fibers Bamboo fibers Wheat straw fibers	46.4 41.8 39.8	-	-	9
Wood fibers	46.7	-	-	31
Daphne papyracea *Grew optiva*	38.63 35.23	-	-	29
Acetobacter xylinum cell wall	-	AgNPs	E. coli (2) S. aureus (3.5)	42
Pine pulp	-	AgNPs	E. coli (4.26) S. aureus (1.41)	43
Poplar wood chips	47.9	AgNPs	E. coli (> 5) S. aureus (> 3)	44
Eulaliposis binata	31.34	AgNPs	E. coli (8.0) B. subtilis (7.0) C. albicans (8.5)	37
Alnus nepalensis and *Coriaria nepalensis*	37.0 & 25.53	AgNPs	E. coli (7.4 & 7.1) B. subtilis (4.5 & 4.3)	This work.

4. Conclusions and recommendations

This study successfully demonstrated the extraction and characterization of cellulose, hemicellulose, and lignin from *Alnus nepalensis* and *Coriaria nepalensis*, along with the functionalization of cellulose with silver nanoparticles to develop antimicrobial nanocomposites. Structural analyses (FTIR, XRD) confirmed the successful isolation of lignocellulosic materials, while FE-SEM revealed interconnected nanofibrillar networks in both ANC and CNC. The incorporation of AgNPs via chemical reduction preserved the native cellulose structure while imparting functional properties, as evidenced by Ultraviolet-Visible (UV-Vis) spectroscopy and XRD. The nanocomposites exhibited significant antimicrobial activity against both Gram-positive and Gram-negative bacteria, with inhibition zones comparable to pure AgNPs and the antibiotic control. Notably, the nanocomposites showed enhanced efficacy against *E. coli*, likely due to the synergistic effects of AgNPs in microbial membrane disruption and the biocompatibility of cellulose.

These findings highlight sustainable material development, i.e., the extraction of high-purity cellulose from *A. nepalensis* and *C. nepalensis*, and functional nanocomposite design, i.e., the incorporation of AgNPs in the cellulose matrix to form a nanocomposite with retained antimicrobial potency. Future work should optimize AgNP loading ratios to enhance antimicrobial specificity and assess long-term stability. The demonstrated efficacy of these nanocomposites positions them as promising candidates for biomedical and industrial applications, merging sustainability and functionality.

Acknowledgements

The authors are grateful to Amrit Campus, Tribhuvan University, Kathmandu, Nepal, for providing laboratory facilities and Himalayan Laboratory Pvt. Ltd. for testing antimicrobial susceptibility.

Conflict of interest

The authors declare that there is no conflict of interest.

References

[1] da Silva Braga, R.; Poletto, M. Preparation and characterization of hemicellulose films from sugarcane bagasse. *Materials* **2020,** *13*(4), 941. https://doi.org/10.3390/ma13040941.

[2] Segers, B.; Nimmegeers, P.; Spiller, M.; Tofani, G.; Jasiukaitytė-Grojzdek, E.; Dace, E.; Kikas, T.; Marchetti, J. M.; Rajić, M.; Yildiz, G.; et al. Lignocellulosic biomass valorisation: a review of feedstocks, processes and potential value chains and their implications for the decision-making process. *RSC Sustain.* **2024,** *2*(12), 3730-3749. https://doi.org/10.1039/D4SU00342J.

[3] Ojo, A. O. An overview of lignocellulose and its biotechnological importance in high-value product production. *Fermentation* **2023,** *9*(11), 990. https://doi.org/10.3390/fermentation9110990.

[4] Mondragon, G.; Fernandes, S.; Retegi, A.; Peña, C.; Algar, I.; Eceiza, A.; Arbelaiz, A. A common strategy to extracting cellulose nanoentities from different plants. *Ind. Crops Prod.* **2014,** *55*, 140-148. https://doi.org/10.1016/j.indcrop.2014.02.014.

[5] Brinchi, L.; Cotana, F.; Fortunati, E.; Kenny, J. M. Production of nanocrystalline cellulose from lignocellulosic biomass: technology and applications. *Carbohydr. Polym.* **2013,** *94*(1), 154-169. https://doi.org/10.1016/j.carbpol.2013.01.033.

[6] Li, T.; Chen, C.; Brozena, A. H.; Zhu, J. Y.; Xu, L.; Driemeier, C.; Dai, J.; Rojas, O. J.; Isogai, A.; Wågberg, L.; et al. Developing fibrillated cellulose as a sustainable technological material. *Nature* **2021,** *590*(7844), 47-56. https://doi.org/10.1038/s41586-020-03167-7.

[7] Chen, H. Chemical composition and structure of natural lignocellulose. In *Biotechnology of Lignocellulose: Theory and Practice*; Springer: Dordrecht, 2014; pp 25-71. https://doi.org/10.1007/978-94-007-6898-7_2.

[8] Chen, W.; Yu, H.; Liu, Y.; Hai, Y.; Zhang, M.; Chen, P. Isolation and characterization of cellulose nanofibers from four plant cellulose fibers using a chemical-ultrasonic process. *Cellulose* **2011,** *18*(2), 433-442. https://doi.org/10.1007/s10570-011-9497-z.
[9] Flauzino Neto, W. P. F. Morphological investigation of cellulose nanocrystals and nanocomposite applications. Ph.D. Thesis, Université Grenoble Alpes, Universidade Federal de Uberlândia, 2017.
[10] Wyman, C. E.; Decker, S. R.; Himmel, M. E.; Brady, J. W.; Skopec, C. E.; Viikari, L. Hydrolysis of cellulose and hemicellulose. In *Polysaccharides: Structural Diversity and Functional Versatility*; Dumitriu, S., Ed.; CRC Press: Boca Raton, 2005; pp 995-1033. https://doi.org/10.1201/9781420030822.CH43.
[11] Youssefian, S.; Rahbar, N. Molecular origin of strength and stiffness in bamboo fibrils. *Sci. Rep.* **2015,** *5*(1), 11116. https://doi.org/10.1038/srep11116.
[12] Zambrano, F.; Starkey, H.; Wang, Y.; de Assis, C. A.; Venditti, R.; Pal, L.; Jameel, H.; Hubbe, M. A.; Rojas, O. J.; Gonzalez, R. Using micro- and nanofibrillated cellulose as a means to reduce weight of paper products: a review. *BioResources* **2020,** *15*(2), 4553-4590. https://doi.org/10.15376/BIORES.15.2.ZAMBRANO.
[13] Lavoine, N.; Desloges, I.; Dufresne, A.; Bras, J. Microfibrillated cellulose-its barrier properties and applications in cellulosic materials: a review. *Carbohydr. Polym.* **2012,** *90*(2), 735-764. https://doi.org/10.1016/j.carbpol.2012.05.026.
[14] Sun, X.-F.; Sun, R.; Fowler, P.; Baird, M. S. Extraction and characterization of original lignin and hemicelluloses from wheat straw. *J. Agric. Food Chem.* **2005,** *53*(4), 860-870. https://doi.org/10.1021/jf040456q.
[15] Farhat, W.; Venditti, R.; Quick, A.; Taha, M.; Mignard, N.; Becquart, F.; Ayoub, A. Hemicellulose extraction and characterization for applications in paper coatings and adhesives. *Ind. Crops Prod.* **2017,** *107*, 370-377. https://doi.org/10.1016/j.indcrop.2017.05.055.
[16] Watkins, D.; Nuruddin, M.; Hosur, M.; Tcherbi-Narteh, A.; Jeelani, S. Extraction and characterization of lignin from different biomass resources. *J. Mater. Res. Technol.* **2015,** *4*(1), 26-32. https://doi.org/10.1016/j.jmrt.2014.10.009.
[17] Jampa, S.; Puente-Urbina, A.; Ma, Z.; Wongkasemjit, S.; Luterbacher, J. S.; van Bokhoven, J. A. Optimization of lignin extraction from pine wood for fast pyrolysis by using a γ-valerolactone-based binary solvent system. *ACS Sustain. Chem. Eng.* **2019,** *7*(4), 4058-4068. https://doi.org/10.1021/acssuschemeng.8b05498.
[18] Shi, Z.; Xu, G.; Deng, J.; Dong, M.; Murugadoss, V.; Liu, C.; Shao, Q.; Wu, S.; Guo, Z. Structural characterization of lignin from *D. sinicus* by FTIR and NMR techniques. *Green Chem. Lett. Rev.* **2019,** *12*(3), 235-243. https://doi.org/10.1080/17518253.2019.1627428.
[19] Haile, A.; Gebino, G.; Tesfaye, T.; Mengie, W.; Ayele, M.; Abuhay, A.; Yilie, D. Utilization of non-wood biomass for pulp manufacturing in paper industry: case of Ethiopia. *Biomass Conv. Bioref.* **2023,** *13*(9), 7441-7459. https://doi.org/10.1007/s13399-021-01424-x.
[20] Vicente, A. T.; Araújo, A.; Mendes, M. J.; Nunes, D.; Oliveira, M. J.; Sanchez-Sobrado, O.; Ferreira, M. P.; Águas, H.; Fortunato, E.; Martins, R. Multifunctional cellulose-paper for light harvesting and smart sensing applications. *J. Mater. Chem. C* **2018,** *6*(13), 3143-3181. https://doi.org/10.1039/C7TC05271E.
[21] McDougall, G. J.; Morrison, I. M.; Stewart, D.; Weyers, J. D. B.; Hillman, J. R. Plant fibres: botany, chemistry and processing for industrial use. *J. Agric. Food Chem.* **1993,** *62*(1), 1-20. https://doi.org/10.1002/jsfa.2740620102.
[22] Kharal, D. K.; Oli, B. N.; Poudel, I. Distribution and availability of raw materials for production of Nepali handmade paper from *Daphne* species in Darchula district, Nepal. *Banko Janakari* **2011,** *21*(2), 24-30. https://doi.org/10.3126/banko.v21i2.9126.
[23] Poudyal, A. S. Sustainability of local hand-made paper (Nepali kagat) enterprises: a case study of Dolakha district. *J. For. Livelihood* **2004,** *4*(1), 64-69. https://doi.org/10.3126/jfl.v4i1.59773.
[24] Noshiro, S.; Suzuki, M.; Joshi, L. Ecological wood anatomy of *Alnus nepalensis* (Betulaceae) in East Nepal. *J. Plant Res.* **1994,** *107*(4), 399-408. https://doi.org/10.1007/BF02344063.
[25] Xia, C.; Zhao, W.; Wang, J.; Sun, J.; Cui, G.; Zhang, L. Progress on geographical distribution, driving factors and ecological functions of Nepalese alder. *Diversity* **2023,** *15*, 59. https://doi.org/10.3390/d15010059.
[26] Ahmad, A.; Khan, A.; Kumar, P.; Bhatt, R. P.; Manzoor, N. Antifungal activity of *Coriaria nepalensis* essential oil by disrupting ergosterol biosynthesis and membrane integrity against Candida. *Yeast* **2011,** *28*(8), 611-617. https://doi.org/10.1002/yea.1890.
[27] Kumar, P.; Bhatt, R. P.; Singh, L.; Sati, O. P.; Khan, A.; Ahmad, A. Antimicrobial activities of essential oil and methanol extract of *Coriaria nepalensis*. *Nat. Prod. Res.* **2011,** *25*(11), 1074-1081. https://doi.org/10.1080/14786419.2010.529545.
[28] Guo, L.; Qiang, T.; Ma, Y.; Wang, K.; Du, K. Optimisation of tannin extraction from *Coriaria nepalensis* bark as a renewable resource for use in tanning. *Ind. Crops Prod.* **2020,** *149*, 112360. https://doi.org/10.1016/

j.indcrop.2020.112360.
[29] Rajaure, A.; Chaudhary, P.; Gharti, S.; Sigdel, A.; Pathak, I.; Prasad, M. K.; Oli, H. B.; Bhattarai, D. P. Extraction of cellulose from stem and bark of *Daphne papyracea* and *Grewia optiva* plants and its characterization. *Amrit Res. J.* **2023,** *4*(1), 21-29. https://doi.org/10.3126/arj.v4i1.61184.
[30] Silverstein, R. M.; Bassler, G. C. Spectrometric identification of organic compounds. *J. Chem. Educ.* **1962,** *39*(11), 546. https://doi.org/10.1021/ed041pA806.1.
[31] Hospodarova, V.; Singovszka, E.; Stevulova, N. Characterization of cellulosic fibers by FTIR spectroscopy for their further implementation to building materials. *Am. J. Anal. Chem.* **2018,** *9*(6), 303-310. https://doi.org/10.4236/ajac.2018.96023.
[32] Ahmad, N.; Tayyeb, D.; Ali, I.; Alruwaili, N. K.; Ahmad, W.; ur Rehman, A.; Khan, A. H.; Iqbal, M. S. Development and characterization of hemicellulose-based films for antibacterial wound-dressing application. *Polymers* **2020,** *12*(3), 548. https://doi.org/10.3390/polym12030548.
[33] Nayem, S. M. A.; Sultana, N.; Haque, M. A.; Miah, B.; Hasan, M. M.; Islam, T.; Hasan, M. M.; Awal, A.; Uddin, J.; Aziz, M. A.; et al. Green synthesis of gold and silver nanoparticles by using *Amorphophallus paeoniifolius* tuber extract and evaluation of their antibacterial activity. *Molecules* **2020,** *25*(20), 4773. https://doi.org/10.3390/molecules25204773.
[34] Vijayakumar, S.; Chen, J.; Amarnath, M.; Tungare, K.; Bhori, M.; Divya, M.; González-Sánchez, Z. I.; Durán-Lara, E. F.; Vaseeharan, B. Cytotoxicity, phytotoxicity, and photocatalytic assessment of biopolymer cellulose-mediated silver nanoparticles. *Colloids Surf. A* **2021,** *628*, 127270. https://doi.org/10.1016/j.colsurfa.2021.127270.
[35] Zhao, D.; Yang, F.; Dai, Y.; Tao, F.; Shen, Y.; Duan, W.; Zhou, X.; Ma, H.; Tang, L.; Li, J. Exploring crystalline structural variations of cellulose during pulp beating of tobacco stems. *Carbohydr. Polym.* **2017,** *174*, 146-153. https://doi.org/10.1016/j.carbpol.2017.06.060.
[36] Zope, G.; Goswami, A.; Kulkarni, S. Isolation and characterization of cellulose nanocrystals produced by acid hydrolysis from banana pseudostem. *BioNanoSci.* **2022,** *12*(2), 463-471. https://doi.org/10.1007/s12668-022-00960-8.
[37] Rajaure, A.; Shreesa, K. C.; Rijal, S.; Adhikari, S.; Chaudhary, S.; Subedi, B.; Sigdel, A.; Prasad, M. K.; Oli, H. B.; Bhattarai, D. P. Incorporation of silver nanoparticle in cellulose nanocrystal extracted from *Eulaliopsis binata* leaf to enhance its antimicrobial activity. *Am. Res. J.* **2024,** *5*(1), 40-48. https://doi.org/10.3126/arj.v5i1.73523.
[38] Meng, Y. A sustainable approach to fabricating Ag nanoparticles/PVA hybrid nanofiber and its catalytic activity. *Nanomaterials* **2015,** *5*(2), 1124-1135. https://doi.org/10.3390/nano5021124.
[39] Priyadharshini, R. I.; Prasannaraj, G.; Geetha, N.; Venkatachalam, P. Microwave-mediated extracellular synthesis of metallic silver and zinc oxide nanoparticles using macro-algae (*Gracilaria edulis*) extracts and its anticancer activity against human PC3 cell lines. *Appl. Biochem. Biotechnol.* **2014,** *174*(8), 2777-2790. https://doi.org/10.1007/s12010-014-1225-3.
[40] Mehta, B. K.; Chhajlani, M.; Shrivastava, B. D. Green synthesis of silver nanoparticles and their characterization by XRD. *J. Phys.: Conf. Ser.* **2017,** *836*, 012050. https://doi.org/10.1088/1742-6596/836/1/012050.
[41] Giri, A. K.; Jena, B.; Biswal, B.; Pradhan, A. K.; Arakha, M.; Acharya, S.; Acharya, L. Green synthesis and characterization of silver nanoparticles using *Eugenia roxburghii* DC. extract and activity against biofilm-producing bacteria. *Sci. Rep.* **2022,** *12*, 8383. https://doi.org/10.1038/s41598-022-12484-y.
[42] Maneerung, T.; Tokura, S.; Rujiravanit, R. Impregnation of silver nanoparticles into bacterial cellulose for antimicrobial wound dressing. *Carbohydr. Polym.* **2008,** *72*(1), 43-51. https://doi.org/10.1016/j.carbpol.2007.07.025.
[43] Li, J.; Kang, L.; Wang, B.; Chen, K.; Tian, X.; Ge, Z.; Zeng, J.; Xu, J.; Gao, W. Controlled release and long-term antibacterial activity of dialdehyde nanofibrillated cellulose/silver nanoparticle composites. *ACS Sustainable Chem. Eng.* **2019,** *7*(1), 1146-1158. https://doi.org/10.1021/acssuschemeng.8b04799.
[44] Chen, Q.-Y.; Xiao, S.-L.; Shi, S. Q.; Cai, L.-P. A one-pot synthesis and characterization of antibacterial silver nanoparticle-cellulose film. *Polymers* **2020,** *12*(2), 440. https://doi.org/10.3390/polym12020440.